CONF-9609114--1

DEVELOPMENT OF A SHALLOW-FLAW FRACTURE ASSESSMENT METHODOLOGY FOR NUCLEAR REACTOR PRESSURE VESSELS

B. R. Bass[#], J. W. Bryson[#], T. L. Dickson[#], W. J. McAfee[#], and W. E. Pennell[#]

Shallow-flaw fracture technology is being developed within the Heavy-Section Steel Technology (HSST) Program for application to the safety assessment of radiation-embrittled nuclear reactor pressure vessels (RPVs) containing postulated shallow flaws. Cleavage fracture in shallow-flaw cruciform beam specimens tested under biaxial loading at temperatures in the lower transition temperature range was shown to be strain-controlled. A strain-based dual-parameter fracture toughness correlation was developed and shown to be capable of predicting the effect of crack-tip constraint on fracture toughness for strain-controlled fracture. A probabilistic fracture mechanics (PFM) model that includes both the properties of the inner-surface stainless-steel cladding and a biaxial shallow-flaw fracture toughness correlation gave a reduction in probability of cleavage initiation of more than two orders of magnitude from an ASME-based reference case.

INTRODUCTION

The loading conditions generated during a pressurized-thermal-shock (PTS) transient are of primary interest for the structural integrity assessment of an RPV pressure boundary. A PTS loading transient produces biaxial pressure and thermal stress fields in the wall of an RPV. Thermal stresses are highest adjacent to the inner surface of the vessel where the effects of irradiation embrittlement and transient temperatures combine to produce the maximum reduction in the material fracture toughness. The net result of this combination of conditions is that the majority of predicted crack initiations originate from shallow flaws located on the inner surface of the RPV (Selby et al (1)). The dominant influence of shallow surface flaws generates the need for a shallow-flaw fracture assessment methodology that incorporates /1/ the effects of reduced crack-tip constraint on material fracture toughness associated with shallow flaws; /2/ the effects of prototypical biaxial stress states on measured fracture toughness data for shallow flaws; /3/ dual-parameter fracture correlations for predicting material fracture toughness of shallow flaws in a biaxial stress field; and /4/ the effects of an inner-surface thin layer of stainless-steel cladding on fracture behavior of shallow surface flaws. This paper provides an overview of recent developments in shallow-flaw fracture technology for RPVs resulting from HSST Program research in these areas.

[#] Oak Ridge National Laboratory, Oak Ridge, Tennessee

DISCLAIMER

FRACTURE TOUGHNESS DATA

Fracture toughness tests have been performed on single-edge notch bend (SENB) test specimens using both deep and shallow flaws (Theiss et al (2), Bass et al (3), and Link and Joyce (4)). Beams tested by ORNL were fabricated from A 533 Grade B Class 1 (A 533 B) material and were nominally 100 mm deep (2). Clad beams cut with a 230 mm square cross section from the RPV of a canceled nuclear plant were tested under the HSST Program (3). Additional shallow-flaw fracture-toughness data for A 533 B material were generated by the Naval Surface Warfare Center (NSWC), in Annapolis, Maryland (4). The NSWC tests were also conducted using large (B = 89 mm, W = 83 mm) SENB specimens. Figure 1 shows that the shallow-flaw fracture-toughness data from all sources form a homogeneous population when plotted as a function of temperature normalized to the nil-ductility temperature (T-NDT). The lower-bound curves for the deep- and shallow-flaw data were shown to be similar (Pennell et al (5)), but the mean fracture-toughness and scatter of data are significantly higher for shallow flaws than for deep flaws.

Pressure and thermal gradient loadings both produce biaxial stress fields in the wall of an RPV. One of the principal stresses is aligned parallel to the crack front of a shallow surface flaw oriented in the longitudinal direction. There is no counterpart of this far-field out-of-plane stress in fracture-toughness tests performed using SENB test specimens with uniaxial loading. Shallow-flaw fracture-toughness of RPV material has been shown to be higher than the deep-flaw fracture-toughness because of the relaxation of crack-tip constraint (2). The far-field out-of-plane stress has the potential to increase stress triaxiality (constraint) at the crack-tip, and thereby reduce the shallow-flaw fracture-toughness enhancement. Therefore, effects of biaxial-loading must be factored into application of shallow-flaw fracture-toughness data to the probabilistic analysis of RPV integrity under PTS loading.

An initial series of biaxial fracture toughness tests (Pennell et al (6)) has been completed using test specimens of the cruciform design shown in Figure 2. This cruciform specimen was specially developed at ORNL to permit the controlled application of biaxial loading, which results in controlled variations of crack-tip constraint for shallow surface flaws. The biaxial load ratio is defined as P_T/P_L, where P_T is the total load applied to the transverse beam arms and P_L is the total load applied to the longitudinal arms. Tests were run with P_T/P_L ratios of 0.0, 0.6, and 1.0. K_{Jc} data from the biaxial tests are shown in Figure 3, plotted as functions of the biaxiality ratio P_T/P_L. The plot shows a decrease in the lower-bound shallow-flaw fracture-toughness with increasing biaxiality ratios. The data also indicate a trend of decreasing data scatter at a stress ratio of 0.6 when compared with the data scatter observed in both the uniaxial ($P_T/P_L = 0$) SENB shallow-flaw tests (see Figure 1) and the biaxial shallow-flaw tests at a P_T/P_L loading ratio of 1.0.

The HSST Program is conducting a series of biaxial cruciform tests (5), (6) to investigate the behavior of shallow, finite–length, through–clad surface flaws where the cladding, temperature, and biaxial load ratio are the primary independent variables. The latter test series is utilizing the same source material as that used for the ORNL full–thickness clad beams specimens (3). In these clad cruciform specimens, the test flaw leading edge passes through the clad material, the HAZ, and, for flaws deeper than approximately 10 mm, into the RPV shell base material.

These tests will help define an envelope of flaw sizes for which cleavage initiation will not be expected under severe PTS type loading. Such an envelope will allow exclusion of such a family of small flaws from probabilistic analyses, potentially contributing to a reduction in the calculated conditional probability of RPV failure.

DUAL-PARAMETER TOUGHNESS CORRELATIONS

Crack-tip constraint is the term used to describe conditions that influence the hydrostatic component of the crack-tip stress field. Dual-parameter fracture-toughness corrections and correlations have been proposed to provide a quantitative assessment of the effect of reduction of crack-tip constraint on fracture-toughness. Stress-based dual-parameter methodologies include the J-A_{σ} fracture-toughness scaling procedure proposed by Dodds et al (7). This methodology utilizes the effect of crack-tip constraint on the in-plane stresses at the crack tip to infer the effect of constraint on fracture-toughness. Prior investigations of biaxial loading effects have concluded that out-of-plane biaxial loading has little effect on in-plane stresses at the crack tip, but does influence the width of the crack-tip plastic zone in the direction of crack propagation (5), (6). Recent elastic-plastic finite element analyses of the biaxial cruciform specimen, using a model with a highly refined treatment of the crack-tip region, have confirmed these conclusions (6). In Figure 4, far-field stress biaxiality is seen to have little effect on the in-plane stresses near the crack tip of the ORNL cruciform specimen. Additional analyses (6) have further confirmed that the stress-based constraint correction procedure described in reference (7) cannot predict the observed effects of biaxial loading on shallow-flaw fracture-toughness.

Wells (8) proposed that initiation of cleavage fracture is controlled by strains in the crack-tip region reaching a critical value. Adopting a strip-yield model, he studied the hypothesis that initiation of brittle fracture is uniquely determined by a critical value, δ_c, of the crack-tip opening displacement (CTOD). For plane stress conditions, he developed relationships between CTOD, δ, the plastic zone width in the plane of the crack, R_{pl}, and overall plastic strain, for loading conditions that range from below to above general yielding. Beyond general yielding, he postulated that δ becomes proportional to the plastic strain taken over some gauge length spanning the fully plastic area of the specimen.

As previously noted, a second (or dual) correlation parameter must also be introduced into the cleavage fracture model to quantify loss-of-constraint or departure from small-scale yielding conditions. The case for using R_{pl} in a strain-based fracture-toughness correlation derives from the observation that the CTOD (δ) is a function of R_{pl} and that this relationship is constraint-dependent. The δ vs R_{pl} relationship has been studied by ORNL (5) for general beyond-plane-strain boundary conditions, for both contained and uncontained yielding, using test data from the biaxial cruciform testing program. A linear relationship between $\sqrt{\delta_c}$ and $\ln(R_{pl})$ was determined from 3-D finite element analysis of the biaxial test results at cleavage fracture initiation and is given by

$$\sqrt{\delta_C} = 1.909 + 0.189 \ln(R_{pl}) \qquad (1)$$

and shown in Figure 5. Also in Figure 5, the $\sqrt{\delta}$ vs $\ln(R_{pl})$ loading trajectories for three biaxial loading ratios (i.e., P_T/P_L = 0, 0.6, and 1) are superposed on the

fracture toughness locus of Equation 1, together with fracture-toughness data points obtained from the cruciform specimens. These loading trajectories were generated using a modified version of the Wells relation for δ given by (8)

$$\delta = \pi \bar{\varepsilon} R_{pl} \tag{2}$$

where

$$\bar{\varepsilon} = \frac{1}{R_{pl}} \int_0^{R_{pl}} \varepsilon_{33}\, dr \tag{3}$$

In Equation 2, the integrated average of the opening-mode strain, $\bar{\varepsilon}$, taken over R_{pl}, replaces a quantity in reference (8) defined as the overall tensile strain. Variations of $\bar{\varepsilon}$ with longitudinal load, obtained from 3-D finite-element analysis of three biaxial loading cases, P_T/P_L = 0, 0.6, and 1, are given in Figure 6. These $\bar{\varepsilon}$ vs load relations were used in Equation 2, along with calculated values of R_{pl}, to compute the predicted loading trajectories given in Figure 5. These results confirm that a measure of the opening-mode strain field in the near-crack-tip ligament is capable of differentiating among the applied biaxial loading ratios to predict variations in biaxial loading trajectories. The linearity of the K_J vs $\sqrt{\delta}$ relationship is preserved under the full range of biaxial loading ratios. Thus, results for the loading trajectories and fracture toughness locus for the cruciform testing program can be restated in terms of equivalent K_J, K_{Jc} vs $\ln(R_{pl})$ relationships (5).

In Figure 5, intersection of these nonlinear trajectories with the linear toughness locus is governed by the dependence of the trajectories on constraint as influenced by the biaxial loading ratio. Unique toughness values are predicted for the uniaxial (P_T/P_L=0) and biaxial (P_T/P_L =0.6) loading cases. The intersection of the trajectory for equibiaxial (P_T/P_L =1) loading with the toughness locus predicts both low and high toughness values for this loading condition. In fact, these low and high toughness values were realized in tests of the biaxial (P_T/P_L =1) loading case. Uncontained yielding that developed in two of the biaxial (P_T/P_L =1) tests gave high toughness values that were similar to those of the uniaxial loading tests. Collectively, the results depicted in Figures 5-6 confirm that $\ln(R_{pl})$ is a viable second parameter for characterizing strain-controlled fracture.

CLAD MODELING AND BIAXIAL LOADING EFFECTS ON RPV PFM ASSESSMENTS

Commercial nuclear pressurized-water reactors in the United States are constructed with a thin stainless-steel layer of cladding on the inner surface of the vessel. The primary purpose of this cladding is to minimize the volume of corrosion product entering the primary system coolant. Shallow flaws having depths on the order of the combined thickness of the cladding and HAZ dominate the frequency distribution of flaws assumed in probabilistic fracture mechanics (PFM) assessments of RPVs (1). Behavior of these shallow flaws during a PTS transient clearly would be influenced by the material/fracture properties and mechanical interactions associated with the elements that comprise the clad overlay structure.

Analyses of a representative RPV were performed to determine the sensitivity of the conditional probability of crack initiation, designated as P(IIE), to the effects of clad modeling and biaxial loading. Specific refinements were introduced into clad models to take account of a low clad yield stress, and a high clad ductility that precludes initiation in the clad layer. Probabilistic assessments were carried out for axially-oriented finite-length inner surface flaws with an aspect ratio of 2, as well as for 2-D flaws. These PFM analyses considered fifteen discrete flaw depths evenly spaced in a region extending 50 mm from the inner surface of the RPV. The flaw sizes were stochastically simulated as predicted by the Marshall flaw depth distribution function. Loading of the vessel was provided by stylized thermal transients of varying severity that are governed by the final coolant temperature, T_f.

The PFM analyses required that mean-, upper-, and lower-bound fracture-initiation-toughness curves be defined. In the Monte Carlo analysis process, fracture-initiation toughness is stochastically sampled for each simulated initial flaw depth. There is not a sufficient number of experimental shallow-flaw biaxial K_{Jc} data points from which to derive a statistically meaningful mean K_{Jc} curve. Thus, statistically derived lower-bound and mean curves from the shallow-flaw uniaxial K_{Jc} database were adjusted, based on the limited biaxial data, to account for biaxial effects. Figure 7 illustrates the statistically derived mean curve for the shallow-flaw uniaxial K_{Jc} database given in Figure 1. Primary characteristics of this fracture-initiation toughness database are a higher mean value and increased variability, particularly in the transition region. A lower-bound fracture toughness ratio (biaxial/uniaxial) of 0.57 was obtained in HSST program tests with uniaxial and biaxial loading. Therefore, the lower-bound curve for shallow-flaw biaxial loading was established by shifting lower-bound uniaxial curve down by 43 percent. The resulting shallow-flaw biaxial lower-bound K_{Jc} curve is shown in Figure 7. For reference, Figure 7 also includes the ASME K_{Ic} curve. Based on biaxial data in Figure 3, an upper-bound shallow-flaw biaxial curve was derived by adjusting the shallow-flaw uniaxial upper-bound curve down by 3 percent. Also, in Figure 7, the mean curve for shallow-flaw biaxial loading was taken as equidistant between the lower- and upper-bound curves.

The conditional probability of crack initiation vs T_f was computed for a reference case of an embrittled RPV described in reference (5), i.e., an ASME-based fracture toughness correlation, an LEFM model, cladding toughness equal to that of base metal, and a 2-D flaw assumption. Results for this reference case are given as curve 1 in Figure 8. Elements of the reference model were changed separately to determine the corresponding change in conditional probability of initiation for PTS transients of varying severity (all modified cases assumed a semicircular flaw). If the 2-D flaw in the reference model is replaced by a semicircular flaw, a more severe probability of initiation is predicted for a range of higher final coolant temperatures (curve 2 of Figure 8). An approximation for effects of clad plasticity was employed which does not allow the stress in the clad thickness to exceed 379 MPa (model EPFM in Figure 8). High clad ductility is incorporated by not allowing cleavage initiation to occur at any discrete angular location on the crack front that resides in the clad region. Also, fracture toughness correlations based on uniaxial and biaxial shallow-flaw toughness data sets from Figure 7 were considered, in addition to the ASME-based correlations. The combined effects of clad yielding and clad toughness properties provided a decrease in initiation probabilities (from the reference case) of

as much as one order of magnitude over the range of final coolant temperatures (curve 3 in Figure 8). When a uniaxial shallow-flaw toughness correlation is adjusted for biaxial effects, the resultant correlation provides initiation probabilities between one and two orders of magnitude lower than those from the ASME-based correlation (curve 4 in Figure 8). The combined-effects model that includes both the cladding properties and the biaxial shallow-flaw toughness correlation gave the maximum reduction of more than two orders of magnitude from the LEFM-ASME-based correlation (curve 5 in Figure 8).

REFERENCES

(1) Selby, D. L., "Pressurized-Thermal-Shock Evaluation of the Calvert Cliffs Unit 1 Nuclear Power Plant," Oak Ridge National Laboratory, NUREG/CR-4022 (ORNL/TM-9408), 1985.

(2) Theiss, T. H. and Shum, D. K. M., "Experimental and Analytical Investigation of the Shallow-Flaw Effect in Reactor Pressure Vessels," Oak Ridge National Laboratory, NUREG/CR-5886 (ORNL/TM-12115), 1992.

(3) Bass, B. R., Keeney, J. A. and McAfee, W. J., "Assessment of the Fracture Behavior of Weld Material from a Full-Thickness Clad RPV Shell Segment," PVP-Vol. 304, Fatigue and Fracture Mechanics in Pressure Vessels and Piping, ASME 1995, pp. 299-311.

(4) Link, R. E. and Joyce, J. A., "Experimental Investigation of Fracture toughness Scaling Models," Constraint Effects in Fracture: Theory and Applications, American Society Testing Materials, STP 1244, Edited by M. Kirk and A. Bakker, American Society for Testing and Materials, Philadelphia, 1994.

(5) Pennell, W. E., Bass, B. R., Bryson, J. W. Jr., Dickson, T. L. and Merkle, J. G., "Preliminary Assessment of the Effects of Biaxial Loading on Reactor Pressure Vessel Structural-Integrity-Assessment Technology," Proceedings of 4th ASME/JSME International Conference in Nuclear Engineering, New Orleans, LA, March 10-14, 1996.

(6) Pennell, W. E., Bass, B. R., Bryson, J. W. Jr., and McAfee, W. J., "An Interim Report on Shallow-Flaw Fracture Technology Development," PVP-Vol. 304, Fatigue and Fracture Mechanics in Pressure Vessels and Piping, ASME 1995, pp. 91-103.

(7) Dodds, R. H. Jr., Anderson, T. L. and Kirk, M. T., Int. J. of Fracture, Vol. 48, 1991, pp. 1-22.

(8) Wells, A. A., "Application of Fracture Mechanics at and Beyond General Yielding," Report M13/63, British Welding Research Association, British Welding Journal, November 1963, pp. 563-570.

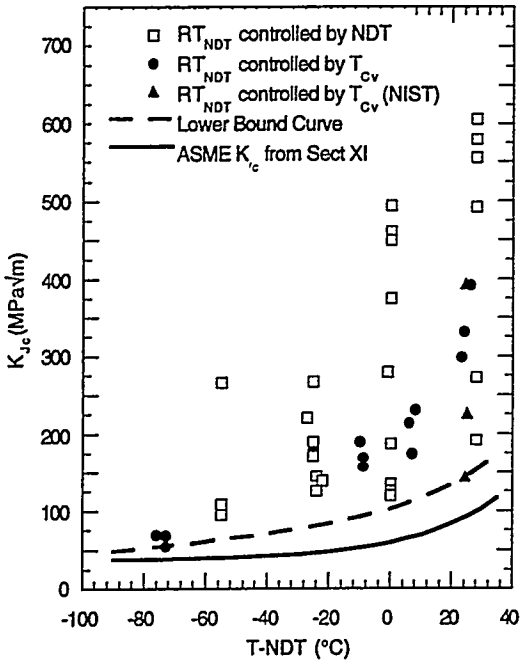

Figure 1 Shallow-flaw toughness data for A533 B Plate and weld material.

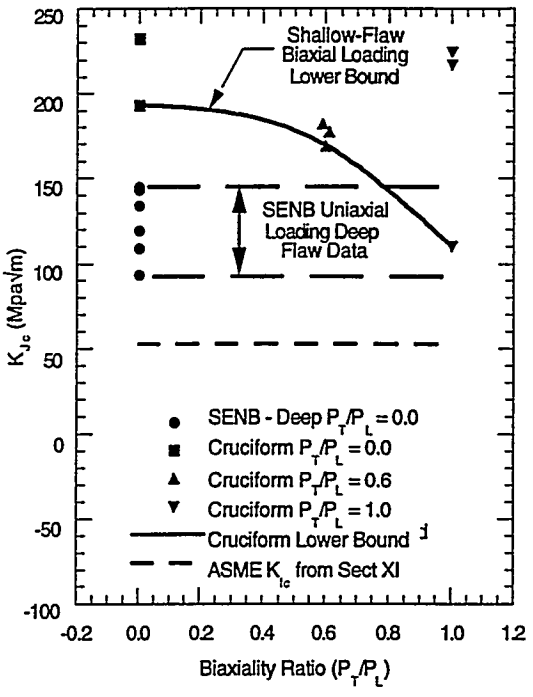

Figure 3 Shallow-flaw toughness data for a single heat of A533 B steel.

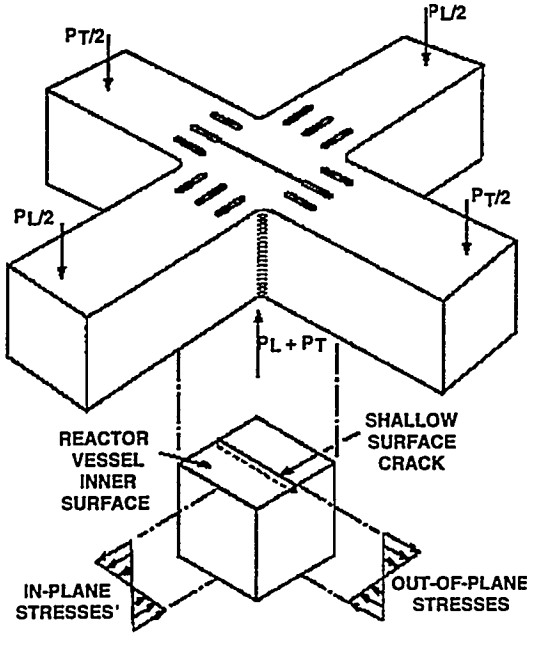

Figure 2 Conceptual features of the cruciform test specimen.

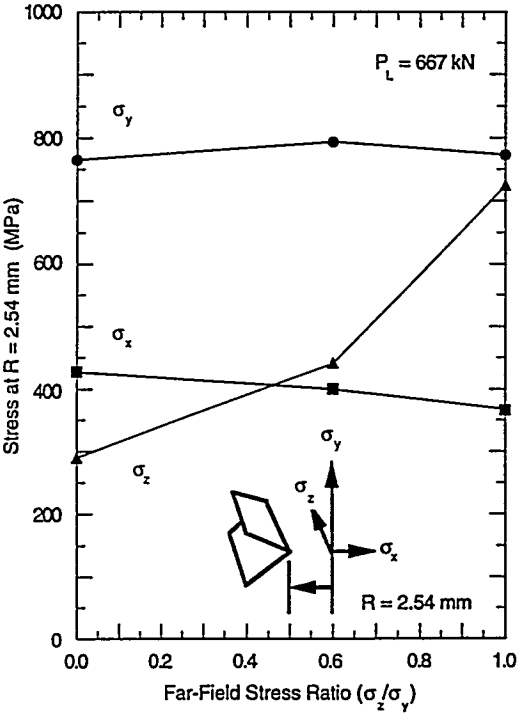

Figure 4 Far-field stress biaxiality effects on in-plane stresses near crack tip.

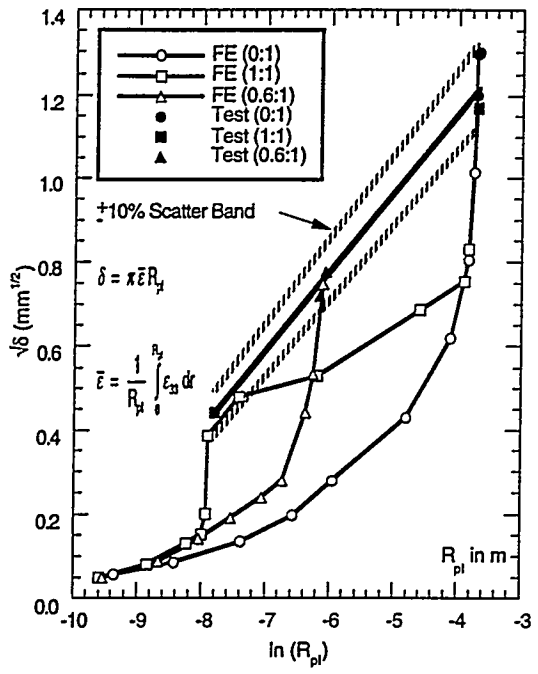

Figure 5 Dependence of $\sqrt{\delta}$ -ln(R_{pl}) loading trajectories on biaxiality ratio.

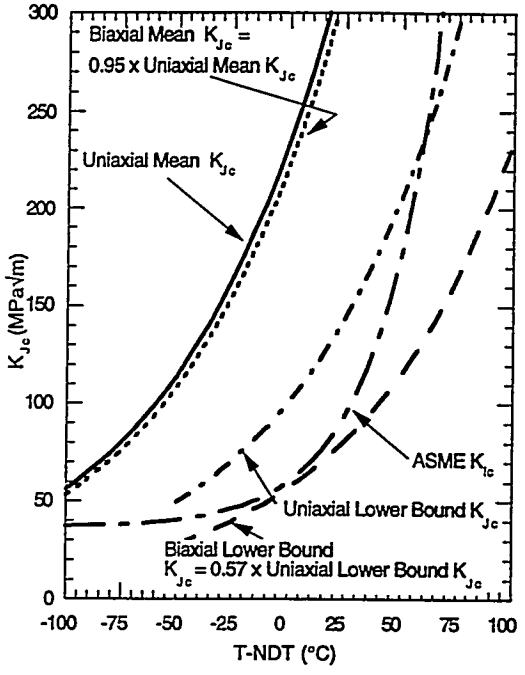

Figure 7 K_{Jc} curves adjusted for effect of biaxiality on shallow-flaw toughness.

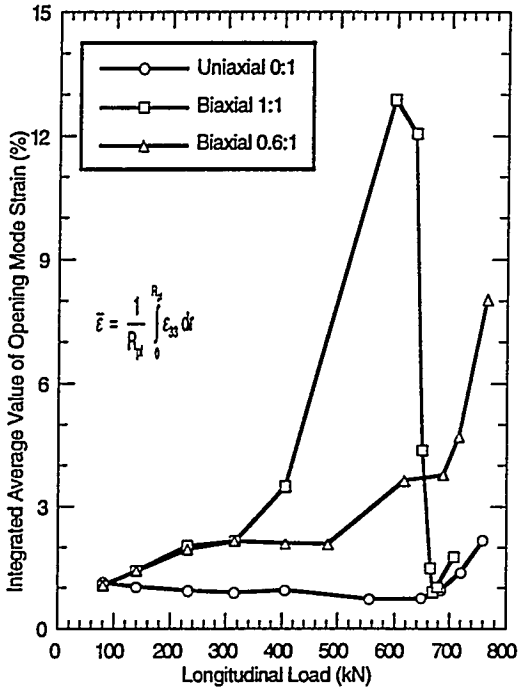

Figure 6 Dependence of opening mode strain on load and biaxiality ratio.

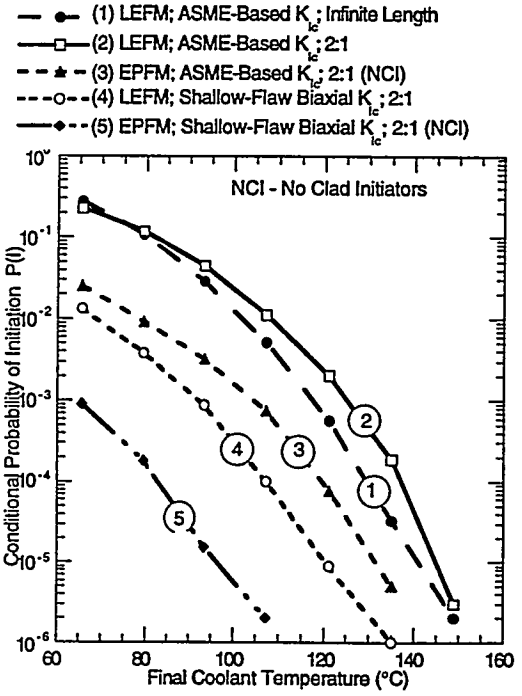

Figure 8 Conditional probability of crack initiation vs final coolant temperature.